A spatially resolved study on the Sn diffusion during the sintering process in the active layer of dye sensitised solar cells

Codrin Andrei [a], **Thomas O'Reilly** [ab] **and Dominic Zerulla** *[ab]
[a]*Strategic Research Cluster in Advanced Biomimetic Materials for Solar Energy Conversion, University College Dublin, Dublin 4, Ireland. E-mail: dominic.zerulla@ucd.ie; Tel: +353 1 716 2507*
[b]*University College Dublin, School of Physics, Dublin 4, Ireland*

Received 5th January 2010 , Accepted 14th April 2010
First published on the web 21st May 2010

Dye sensitised solar cells (DSSCs) use a mesoporous TiO_2 scaffold, typically assisted by an adsorbed dye, as the main active element, responsible for the photon absorption, exciton generation and charge separation functionality. The sintering process employed in the TiO_2 active layer fabrication plays a crucial role in the formation of the nanoparticle scaffold and hence the performance of a dye sensitised solar cell, as it allows the particles to form efficient inter-crystalline electric contacts to provide high electron conductivity. The sintering temperature, with typical values in the range of 450–600 °C, is of particular importance for the formation as it reduces the amount of unwanted organics between the individual crystallites and determines the formation of interfaces between the nanoparticles. Furthermore, the cell design requires a conductive transparent top electrode which is typically made of fluorinated tin oxide or indium tin oxide. Here we report on a highly spatially resolved scanning electron microscopy study including focussed ion beam (FIB) milling and energy dispersive X-ray (EDX) mapping of the distribution of all relevant elements within a DSSC subsequent to a classical sintering process. We find that the above quoted temperatures cause the Sn of the transparent conductive oxide (TCO) to migrate into the TiO_2 scaffold, resulting in unwanted alterations in the composition of the complex scaffold which has a direct effect on the DSSC performance. One potential solution to this problem is the invention of novel concepts in the manufacturing of DSSCs using lower sintering temperatures.

1. Introduction

A dye sensitised solar cell (DSSC) consists of a mesoporous, semiconducting nanoparticle film onto which a monolayer of dye is adsorbed, an electrolyte, a catalytic layer and two electrodes of which one should be transparent (Fig. 1). Other variations to this original setup developed by Grätzel and O'Regan[1] are the focus of recent developments (*e.g.* flexible electrodes,[2] the use of polymers or gel electrolytes[3]) and show promising results for future applications. The working

principle of a DSSC is based on electron injection from an excited state of a dye into the conduction band of a wide band gap semiconductor. Due to its unique properties, titanium dioxide (TiO_2) is one of the most employed semiconductors in the DSSC manufacturing. The process of converting light energy incident on the DSSC to electricity takes place on a molecular level and is therefore, at least in this aspect, similar to photosynthesis in nature; it is a regenerative photoelectrochemical process by way of the electrolyte. The purpose of the dye is to sensitise the TiO_2 layer to the visible and near-infrared part of the solar spectrum, *i.e.* to enhance the wavelength acceptance of TiO_2, as without it the nanoparticle layer would only respond to ultraviolet light according to its band gap.[1] The lowest excited state of the dye must align to the conduction band edge of the semiconductor and the absorption range of the dye should cover the widest range possible, *e.g.* the entire visible spectrum.[4] The effective decrease in the large band gap of the semiconductor (3.2 eV) may be accounted for by assuming the introduction of "new" dye surface states;[1] the range of wavelengths absorbed by a DSSC is governed by this effective band gap. Natural, porphyrin-based sensitizers may be chemically modified to yield higher power conversion efficiencies of up to 7.1%.[5] However, synthetic dyes report the highest efficiencies of up to 11.3% at present[6] and are typically a Ruthenium-based complex.

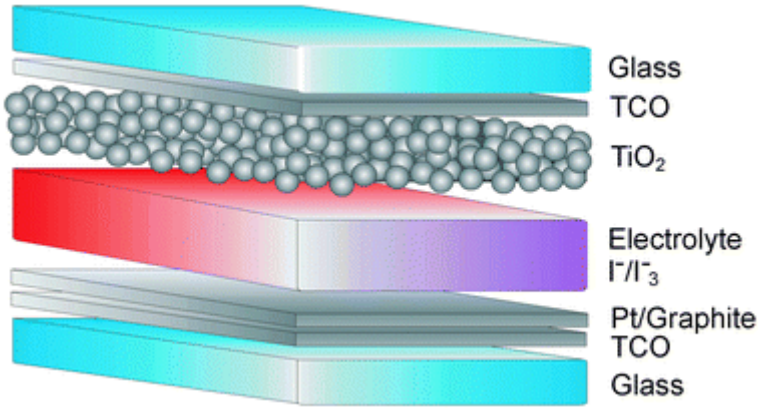

Fig. 1 Schematic of the DSSC design.

The preparation of the DSSC negative electrode includes the sintering of the applied TiO_2 film. This sintering process is required for burning out the organic binders and surfactants, therefore for establishing good electrical contacts between adjacent TiO_2 nanoparticles in the porous layer as well as between the TiO_2 nanoparticles and the transparent conductive layer. The optimal sintering temperature for the semiconducting films forming the negative electrode has been investigated in various literature studies. The TiO_2 sintering temperature of 450 °C was reported to produce good electronic contacts between the nanoparticles and the support substrate, but also between all the nanoparticles that form the scaffold.[7]

In general, the sintering of the TiO_2 films at higher temperatures (*e.g.* 500 °C) translates to higher photocurrents and higher power conversion efficiencies, as opposed to lower temperature (*e.g.* 250 °C).[8] By further increasing the sintering

temperature within a certain band, the crystallinity of the TiO_2 can be enhanced and therefore the performance of the DSSC is also improved.[9] According to Meen *et al.*, the optimum TiO_2 sintering temperature is 600 °C, at which anatase phase forms best. However, if the temperature is increased beyond this point to 700 °C the TiO_2 film turns into the rutile phase completely which is to be avoided in DSSC manufacturing.[10] It should also be mentioned here that temperatures between 500 °C and 600 °C might be the optimum from the "crystallographic standpoint" as reported above, however the glass substrate and the TCO layer might be affected negatively at such high temperatures. An analysis on the optical properties of the SnO_2:F as reported by Iratni *et al.* establishes the idea of the Fermi level shift during the sintering process, which translates into a loss in conductivity and hence, reducing the cell efficiency.[11] The sintering temperature for other important semiconductors employed in the DSSC manufacturing has also been investigated. High porosity ZnO nanocrystalline films can be produced at a sintering temperature of 200 °C, whereas a more compact film is obtained when sintering at 400 °C.[7]

In the present study the DSSC fabrication process followed an accepted combination of methods, as described by O'Regan and Grätzel.[1,12] In order to investigate the effect of the sintering process during the electrode fabrication on the properties of the DSSC, the nanoparticle TiO_2 film was investigated using scanning electron microscopy, focused ion beam, energy dispersive X-ray spectroscopy and current–voltage characteristics analysis.

2. Experimental procedure

The DSSC electrodes are prepared on sheet glass (Nippon Sheet Glass, Solar 4 mm thickness) that has been coated with a transparent conducting oxide (TCO) layer. The TCO layer is fluorine-doped stannic oxide (SnO_2:F) with a sheet resistance of 8 Ω per square. The SnO_2:F is the preferred option for the TCO, as it was published to remain stable at high temperatures, up to 500 °C, during the sintering process required for the production of the DSSCs.[13]The conductive glass substrate is cleaned and rinsed with distilled water, then allowed to dry in a clean environment. The nanostructured TiO_2 electrodes are typically deposited from a TiO_2 nanoparticle colloidal solution, prepared by grinding 12 g of Degussa P25 powder (approx. 70% anatase and 30% rutile) in 20 ml solution of acetylacetone and distilled water. The TiO_2 deposition was achieved using the tape casting technique, also known as the doctor blade technique.[14] After air-drying for 30 min, the TiO_2 coated electrode was formed *via* the sintering process using a high temperature-controllable *Carbolite* oven. The oven was preheated to 450 °C and then the glass slide is placed on a grid and inserted into the oven for 10 min. The temperature is increased to 500 °C and the sample is left for another 10 min within the oven. After this process is finished, the electrode is allowed to cool slowly for 1 h, to prevent the breaking of the glass. The number of potential sensitizers available is vast and may be of a natural or synthetic origin. For the cell, shown in Fig. 2, the TiO_2 nanocrystalline electrode was immersed in a solution of anthocyanin dye that has been chosen as a sensitizer for the cells. The counter electrode is coated with a thin graphite layer, which acts as a catalyst for the

triiodide ⟶ iodide (I_3^-/I^-) regeneration process.[14] The two electrodes are brought together and offset by 5 mm to allow for electrical contacts and held in place with a fixed mechanical pressure. Finally, the DSSC is activated with 50 μl of the iodide–triiodide electrolyte solution, drawn into the cell *via*capillary action.

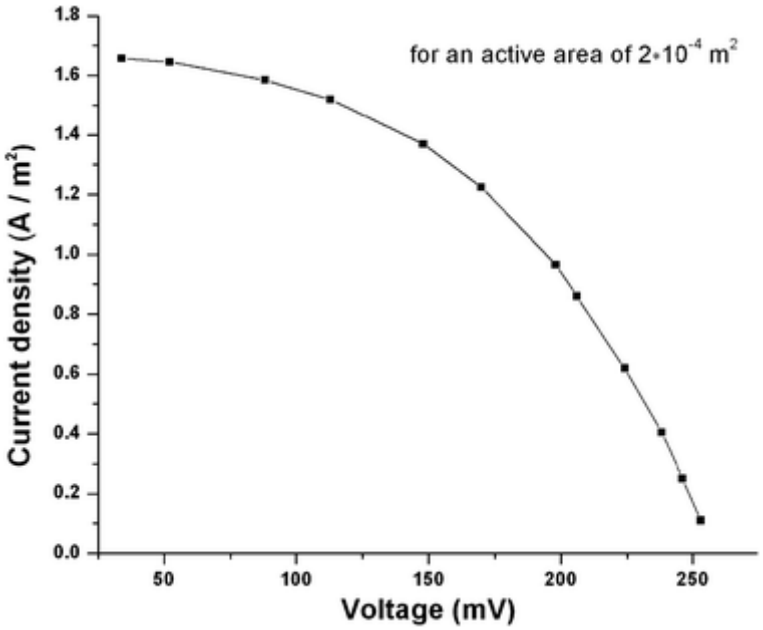

Fig. 2 The current density/voltage curve for variable loads characterizing the performance of the below investigated DSSC.

The DSSCs fabricated as described above show typical performance characteristics, which were characterized by current density–voltage measurements as illustrated in Fig. 2. Based on a standard IV measurements[14] and employing a 1 kW Xenon arc lamp as the light source, a variable resistor was used as an artificial load for the DSSC which was varied from 0 (short circuit, SC) to 10 kΩ resistance in order to show the below current–voltage curve. Additionally, the spectral and temporal response of the cells has been evaluated to confirm their performance.[15]

The structure of the TiO_2 layer that forms the basis of a DSSC was characterized *via* the scanning electron microscopy (SEM) technique. A FEI Quanta 3D® dual beam scanning electron microscope equipped with a highly spatially resolving electron field emission gun, a highly spatially resolving Gallium ion gun and an EDAX Trident XM4 energy dispersive X-ray detector were employed for imaging and depth profiling of the TiO_2 structures, providing a spatial resolution of down to 1.5 nm.

3. Results and discussion

In the following we present details of layer thickness, grain-size and more importantly an insight into the structure of the TiO_2 scaffold subsequent to the above-described sintering process. Fig. 3 shows a typical surface section at a

magnification of 100 000×. It reveals the scaffold structure of the TiO_2 and the depicted pyramid-like nanocrystals indicate that they correspond mainly to the anatase form of the TiO_2. The size of the nanoparticles was measured with high precision and was found to be between 20 nm and 80 nm (some measurements of randomly selected crystals are given in Fig. 3).

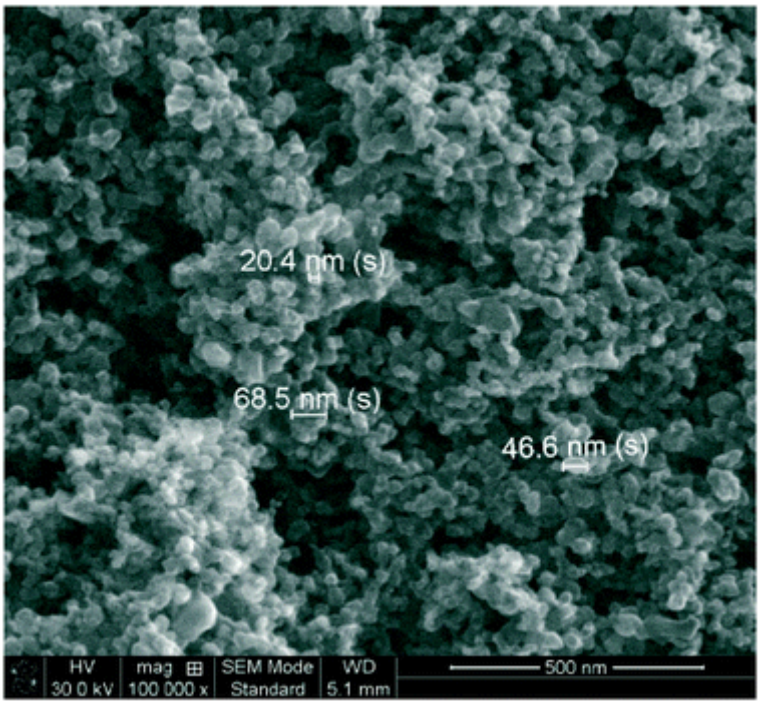

Fig. 3 SEM image of sintered nanoparticle TiO_2 layer, magnification 100 000× and scale bar 500 nm. Average particle size 45 nm.

The SEM images reveal the porous structure of the TiO_2 layer, which is a main asset of the DSSC, as it provides enhanced surface area, dye attachment and thus high photon absorption.

In order to evaluate the absolute thicknesses of the TiO_2 scaffold and the buried TCO layer as well as to get access to the buried TiO_2/TCO and TCO/glass interfaces the focused ion beam (FIB) technique was used to remove a cuboid with dimensions of 20 μm × 30 μm × 20 μm from the DSSC.

Subsequently this section of the DSSC was imaged using scanning electron microscopy at a magnification of 3500× as shown in Fig. 4. Now, the removal of the cube permits access to the relevant DSSC cross-section and the buried interfaces.

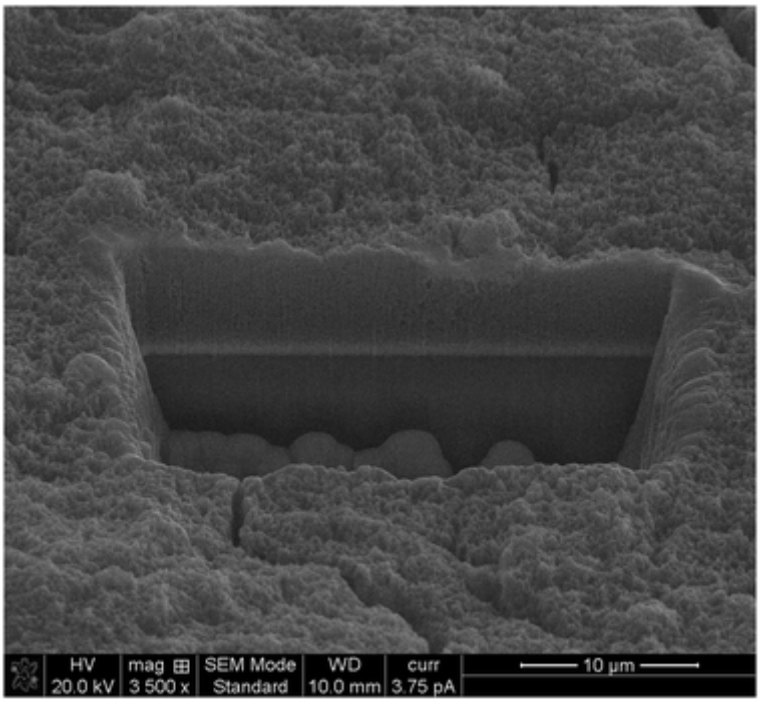

Fig. 4 SEM image subsequent to focussed ion beam milling to evaluate the absolute thickness of the TiO_2 and TCO layers; magnification 3500× and scale bar 10 µm.

Subsequent to the FIB sputtering, electron microscopy at a magnification of 17 500× was used to reveal the layer structure of the DSSC (Fig. 5). The TiO_2 layer was measured to have a depth of ~6.3 µm (6.93 µm–0.65 µm) which indicates a significant shrinking of this layer during the sintering process (reduction factor of 5.5). Such a strong alteration of the TiO_2 thickness illustrates the magnitude of changes induced by the sintering and therefore the importance of the sintering process for the scaffold formation.

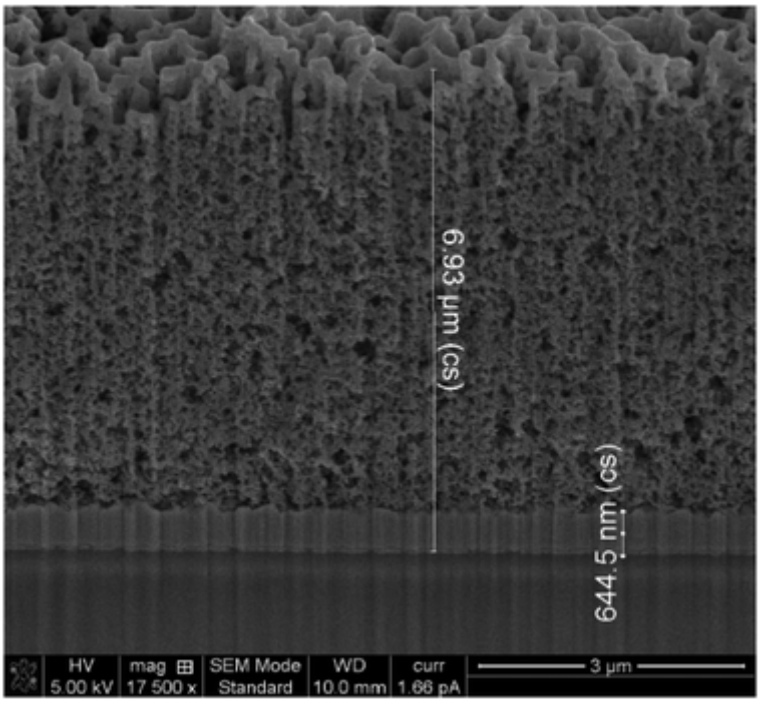

Fig. 5 The nanoparticle TiO_2 layer thickness: 6.3 µm. The TCO layer thickness: 644 nm, magnification 17 500× and scale bar 3 µm.

The next layer that can be clearly identified by its different structure and secondary electrons brightness is the transparent conductive oxide and has a thickness of 645 nm. It should be noted that the vertical channels which appear across the whole DSSC cross-section are an artefact of the FIB removal process. The TCO layer is followed by the glass substrate layer and the two can be clearly distinguished by their brightness. It also shows that the glass composition is not homogenous close to the TCO/glass interface.

More details on the elementary composition of the different layers are provided by an EDX mapping of the cross-sectional area. For this, a platinum layer was deposited on top of the TiO_2 layer, as a conductive, protective layer. Then, the FIB technique was employed again to sputter a small "gap" through the TiO_2 layer, the TCO layer and part of the glass layer similar to the process shown in Fig. 4. Subsequently, the EDX technique was employed to determine the type of each material and the composition of the materials employed (Fig. 6).

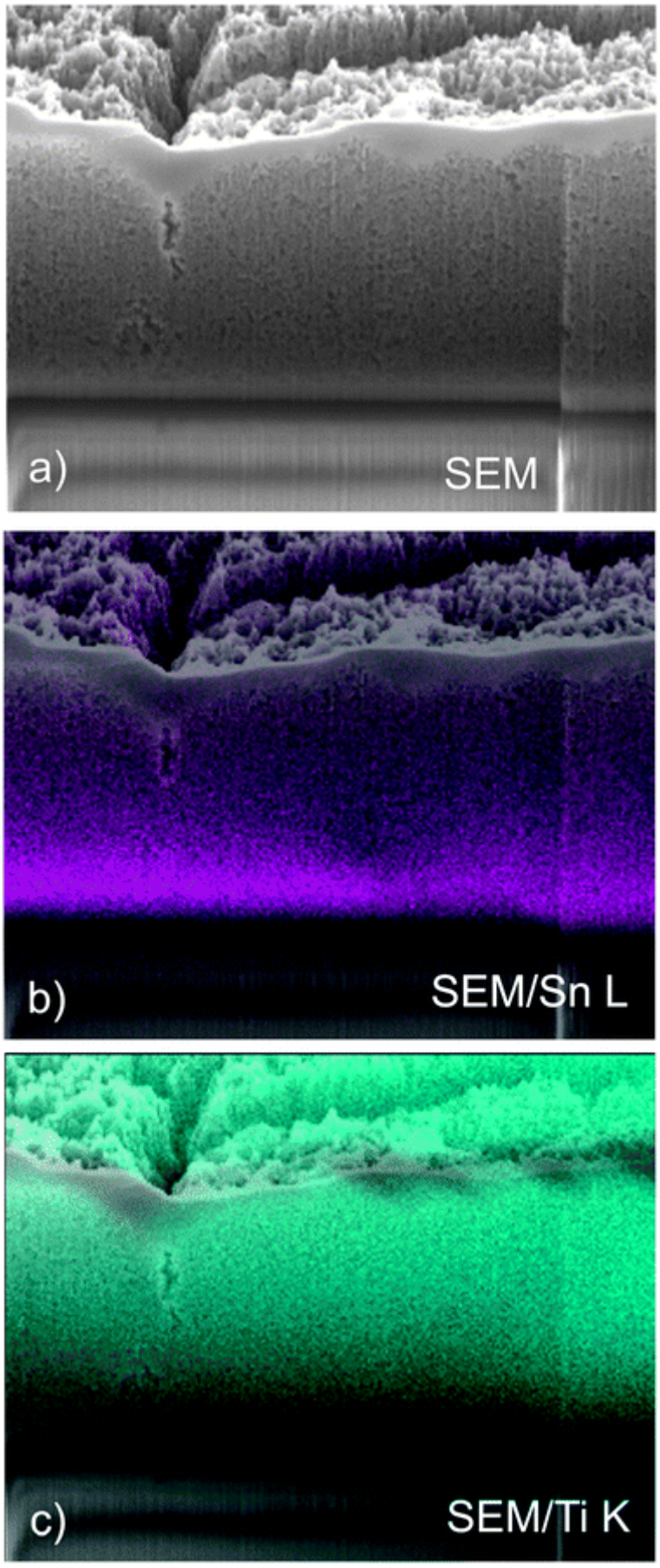

Fig. 6 (a) SEM imaging of the vertical DSSC cross-section; (b) SEM image with superimposed Sn L EDX signal; (c) SEM image with superimposed Ti K EDX signal.

Apart from confirming the layer assignments from Fig. 5, the main result of this analysis is that part of the SnO_2:F, which composes the TCO layer, is diffusing during the sintering process into the TiO_2 scaffold but not into the glass (Fig. 6b).

Fig. 7 shows a compilation of the EDX depth profiles of selected elements (O, Sn, Ti, Si) permitting evaluation of their detailed spatial distributions. The figure indicates that the diffusion seems to be limited to the Sn of the TCO and cannot be found *e.g.* the Si of the glass substrate, since the Si signal (Fig. 7 (right)) is still mostly confined to its original volume. The confinement of the Si as opposed to the diffusion of the TCO layer also suggests that the FIB process is not responsible for the shown diffusion process into the TiO_2 scaffold but the sintering. Further evidence for this statement is given by the fact that one can find Sn also on the surface of the DSSC (away from the FIB milling) in a low but constant concentration.

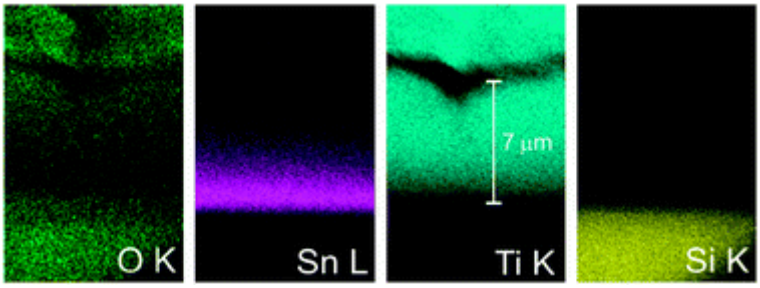

Fig. 7 Comparison of depth distribution of relevant EDX (O K, Sn L, Ti K, Si K) signals.

The Sn (SnO_2) diffusion during the sintering process will influence the electron transport, thus having side-effects on the performance of the cell.

It should be noted that other EDX signals were additionally measured for control purposes, *e.g.* the Ga signal to monitor the unwanted Ga deposition caused by the FIB process. However these signals have been omitted in the article because they have no impact on the discussion.

4. Conclusions and outlook

This article has provided detailed evidence for the temperature induced effects of sintering on a typical DSSC. During this sintering process the TiO_2 layer shrinks by a predictable factor, which allows calculating the final thickness of the TiO_2 layer from its pre-sintered thickness. Furthermore, the EDX analysis permitted the retrieval of a signal from the SnO_2 which migrates into the TiO_2 during the sintering process. The chemical state of the diffused SnO_2 and the effect on the performance of the cell needs further attention because of its unknown effect to the overall performance of DSSCs. These effects may not necessarily be negative, as reported in literature the photocatalytic activity of TiO_2 has been increased when using semiconductor coupled systems like SnO_2/TiO_2,[16–18] in particular doping the anatase lattice with Sn cations enhances the separation of photogenerated pairs.[19] Obviously, as reported in literature, higher

sintering temperatures cause an excellent removal of organic binders and solvents.[10] On the other hand the high temperatures cause the transformation of the anatase TiO_2 into rutile which is undesirable for DSSC performance. Since both effects are competing, it comes as no surprise that different authors, depending on their precise preparation method and duration of sintering, report ideal maximum temperatures between 450 °C–600 °C.

In order to enable a reduction of the sintering temperature and still remove unwanted organics the use of a reductive gas atmosphere has been suggested. Another solution might be the chemical deposition of the TiO_2 scaffold from titanium compounds in organic solvents instead of nanocrystalline suspensions. First experiments of the former indicate the feasibility of such procedures at temperatures as low as 250 °C, however the current state of these experiments still show an inferior efficiency to the here presented DSSCs.

Additional improvement of the cell efficacy is provided by plasmonic enhancement. Some preliminary stages of achievement have already been published.[20–24]

Acknowledgements

We acknowledge and thank the Science Foundation Ireland for their funding of this Strategic Research Cluster in Advanced Biomimetic Materials for Solar Energy Conversion (07/SRC/B1160) and our industry partners: Airtricity, Celtic Catalysts Ltd. and SolarPrint Ltd., for their support of this programme.

Notes and references

1 B. O'Regan and M. Grätzel, *Nature*, 1991, **353**, 737–739 [Links].

2 S. Ito, N.-L. C. Ha, G. Rothenberger, P. Liska, P. Comte, S. M. Zakeeruddin, P. Pechy, M. K. Nazeeruddin and M. Grätzel, *Chem. Commun.*, 2006, 4004–4006 [Links].

3 P. Wang, S. M. Zakeeruddin, J. E. Moser, M. K. Nazeeruddin, T. Sekiguchi and M. Grätzel, *Nat. Mater.*, 2003, **2**, 402–407 [Links].

4 A. Mishra, M. K. R. Fischer and P. Bäuerle, *Angew. Chem., Int. Ed.*, 2009, **48**, 2474–2499 [Links].

5 W. M. Campbell, K. W. Jolley, P. Wagner, K. Wagner, P. J. Walsh, K. C. Gordon, L. Schmidt-Mende, M. K. Nazeeruddin, Q. Wang and M. Grätzel, *J. Phys. Chem. C*, 2007, **111**, 11760–11762 [Links].

6 F. Gao, Y. Wang, D. Shi, J. Zhang, M. Wang, X. Jing, R. Humphry-Baker, P. Wang, S. M. Zakeeruddin and M. Grätzel, *J. Am. Chem. Soc.*, 2008, **130**, 10720–10728 [Links].

7 A. Hagfeldt and M. Grätzel, *Chem. Rev.*, 1995, **95**, 49–68 [Links].

8 P. Balraju, P. Suresh, M. Kumar, M. S. Roy and G. D. Sharma, *J. Photochem. Photobiol., A*, 2009, **206**, 53–63 [Links].

9 M. Zukalová, A. Zukal, L. Kavan, M. K. Nazeeruddin, P. Liska and M. Grätzel, *Nano Lett.*, 2005, **5**, 1789–1792 [Links].

10 T. H. Meen, W. Water, W. R. Chen, S. M. Chao, L. W. Ji and C. J. Huang, *J. Phys. Chem. Solids*, 2009, **70**, 472–476 [Links].

11 R. Tala-Ighil, M. Boumaour, A. Maallemi, K. Melhani and A. Iratni, *Sol. Energy Mater. Sol. Cells*, 2006, **90**, 1797–1814 [Links].

12 M. Grätzel, *Nature*, 2001, **414**, 338–344 [Links].
13 R. G. Gordon, *Mater. Res. Bull.*, 2000, **25**, 52–57 [Links].
14 G. P. Smestad and M. Grätzel, *J. Chem. Educ.*, 1998, **75**, 752–756 [Links].
15 T. O'Reilly, C. Andrei, J. O'Reilly and D. Zerulla, *Proc. SPIE*, 2009, **7410**, 74100L.
16 J. Lin, J. C. Yu, J. Lo and S. K. Lan, *J. Catal.*, 1999, **183**, 368 [Links].
17 S. K. Zheng, T. M. Wang, W. C. Hao and R. Shen, *Vacuum*, 2002, **65**, 155 [Links].
18 Y. Cao, W. Yang, W. Zhang, G. Liu and P. Yue, *New J. Chem.*, 2004, **28**, 218 [Links].
19 B. Xin, D. Ding, Y. Gao, X. Jin, H. Fu and P. Wang, *Appl. Surf. Sci.*, 2009, **255**, 5896–5901 [Links].
20 S. Rehwald, M. Berndt, F. Katzenberg, S. Schwieger, E. Runge, K. Schierbaum and D. Zerulla, *Phys. Rev. B: Condens. Matter Mater. Phys.*, 2007, **76**, 085420 [Links].
21 G. Isfort, K. Schierbaum and D. Zerulla, *Phys. Rev. B: Condens. Matter Mater. Phys.*, 2006, **73**, 033408 [Links].
22 G. Isfort, K. Schierbaum and D. Zerulla, *Phys. Rev. B: Condens. Matter Mater. Phys.*, 2006, **74**, 033404 [Links].
23 B. Ashall, M. Berndt and D. Zerulla, *Appl. Phys. Lett.*, 2007, **91**(20), 203109 [Links].
24 M. Berndt, M. Rohmer, B. Ashall, C. Schneider, M. Aeschlimann and D. Zerulla, *Opt. Lett.*, 2009, **34**(7), 959.